Comparative Proteomics Profiling of a Phospholamban Mutant Mouse Model of Dilated Cardiomyopathy Reveals Progressive Intracellular Stress Responses*[S]

Anthony O. Gramolini,[a,b,c,d,e] Thomas Kislinger,[a,d,f] Rasoul Alikhani-Koopaei,[a] Vincent Fong,[a] Natalie J. Thompson,[a] Ruth Isserlin,[a] Parveen Sharma,[a,b] Gavin Y. Oudit,[b,c] Maria G. Trivieri,[b,c] Ailís Fagan,[g] Anitha Kannan,[h] Desmond G. Higgins,[g] Hendrik Huedig,[i] George Hess,[i] Sara Arab,[b] Jonathan G. Seidman,[j] Christine E. Seidman,[j] Brendan Frey,[h] Marc Perry,[b] Peter H. Backx,[b,c,k] Peter P. Liu,[b] David H. MacLennan,[a,b] and Andrew Emili[a,l]

Defective mobilization of Ca^{2+} by cardiomyocytes can lead to cardiac insufficiency, but the causative mechanisms leading to congestive heart failure (HF) remain unclear. In the present study we performed exhaustive global proteomics surveys of cardiac ventricle isolated from a mouse model of cardiomyopathy overexpressing a phospholamban mutant, R9C (PLN-R9C), and exhibiting impaired Ca^{2+} handling and death at 24 weeks and compared them with normal control littermates. The relative expression patterns of 6190 high confidence proteins were monitored by shotgun tandem mass spectrometry at 8, 16, and 24 weeks of disease progression. Significant differential abundance of 593 proteins was detected. These proteins mapped to select biological pathways such as endoplasmic reticulum stress response, cytoskeletal remodeling, and apoptosis and included known biomarkers of HF (*e.g.* brain natriuretic peptide/atrial natriuretic factor and angiotensin-converting enzyme) and other indicators of presymptomatic functional impairment. These altered proteomic profiles were concordant with cognate mRNA patterns recorded in parallel using high density mRNA microarrays, and top candidates were validated by RT-PCR and Western blotting. Mapping of our highest ranked proteins against a human diseased explant and to available data sets indicated that many of these proteins could serve as markers of disease. Indeed we showed that several of these proteins are detectable in mouse and human plasma and display differential abundance in the plasma of diseased mice and affected patients. These results offer a systems-wide perspective of the dynamic maladaptions associated with impaired Ca^{2+} homeostasis that perturb myocyte function and ultimately converge to cause HF. ***Molecular & Cellular Proteomics 7: 519–533, 2008.***

Cardiomyopathies of diverse etiology impair cardiac muscle function and frequently progress to a convergence point where they induce heart dilatation and overt failure. Although HF[1] is a major source of global morbidity and death in the developed world (1), afflicted patients are typically diagnosed with end stage disease when few effective avenues for restorative intervention remain and clinical outcomes are poor (1). Therefore, innovative preventive and therapeutic measures are needed urgently for more effective early detection, stratification, and treatment of at-risk patients (1). Although considerable progress has been made in the understanding of the mechanistic basis for certain aspects of cardiac dysfunction (2–6), a more complete understanding is required of the key molecular players and biochemical maladaptations associated with disease progression, particularly at the earliest stages of cardiomyopathy that occur prior to clinical presentation.

Previously we reported that an inherited human dilated cardiomyopathy resulted from the conversion of Arg-9 to Cys

From the [a]Banting and Best Department of Medical Research, University of Toronto, Toronto, Ontario M5G 1L6, Canada, [b]Heart and Stroke/Richard Lewar Centre of Excellence, University of Toronto, Toronto, Ontario M5S 3E2, Canada, [c]Department of Physiology, University of Toronto, Toronto, Ontario M5G 1A8, Canada, [g]Conway Institute, University College Dublin, Belfield, Dublin 4, Ireland, [j]Department of Genetics, Harvard Medical School and Howard Hughes Medical Institute, Boston, Massachusetts 02115, [h]Department of Electrical and Computer Engineering, University of Toronto, Toronto, Ontario M5S 3G4, Canada, and [i]Roche Diagnostics, 82377 Penzburg, Germany

Received, May 25, 2007, and in revised form, October 29, 2007
Published, MCP Papers in Press, November 30, 2007, DOI 10.1074/mcp.M700245-MCP200

[1] The abbreviations used are: HF, heart failure; PLN, phospholamban; BNP, brain natriuretic peptide; ANF, atrial natriuretic factor; ACE, angiotensin-converting enzyme; FDR, false discovery rate; GO, Gene Ontology; DPY, dihydropyrimidinase; CIA, co-inertia analysis; PDI, protein-disulfide isomerase; DESM, desmin; IQGAP, Ras GTPase-activating-like protein; CHOP, CIEBP homologous protein; CALU, calumenin; CRTC, calreticulin; POST, periostin; FLN, filamin; ENPL, endoplasmin; PLMN, plasminogen; PLSL, L-plastin; SPTA, spectrin A; SPTB, spectrin B; RTN, reticulocalbin; VIME, vimentin.

in the human phospholamban (*PLN*) gene (PLN-R9C) (7). The onset of dilated cardiomyopathy in affected patients typically commenced during adolescence followed by progressive deterioration in cardiac function leading to crisis and mortality (7). A transgenic mouse model of this mutation showed a remarkably similar cardiac phenotype (7) with the afflicted mice presenting with early onset dilated cardiomyopathy characterized by decreased cardiac contractility and premature death.

In the present study, we used exhaustive gel-free protein profiling and parallel microarray-based mRNA screening techniques to examine temporal changes in the global expression patterns during disease progression in the cardiac ventricular muscle of R9C mutant animals as compared with age-matched healthy controls. Using a p value of 0.05, we deduced significant changes in the levels of 593 of 6190 proteins identified with high confidence. We then used mRNA microarray data together with extensive RT-PCR and immunoblotting for further validation of the 40 proteins that were calculated to be below an empirically corrected false discovery rate (FDR).

Statistically significant over-representation in select Gene Ontology functional categories (GO terms) was detected among both the up- and down-regulated proteins. These GO terms indicated perturbations in cytoskeletal and calcium-binding proteins, alterations in endoplasmic reticulum (ER) stress and apoptosis pathways, and shifts in energy metabolism. We confirmed the activation of apoptosis, and we explored the potential for establishing informative biomarkers of heart disease among the most markedly altered proteins. Overall we established an insightful time course projection of the dynamically changing molecular landscape associated with early stage myocyte dysfunction, midstage cardiac dilatation, and overt end stage HF. The entire processed data set and supporting annotated spectra evidence are fully accessible via a dedicated Website as a platform to support further basic and clinically driven cardiac investigations.

EXPERIMENTAL PROCEDURES

Ventricle Tissue Fractionation and Organelle Isolation—The transgenic phospholamban R9C mutant mice were described previously (7). Male and female mice were analyzed at 8, 16, and 24 weeks by M-mode and Doppler echocardiography for non-invasive assessment of left ventricular function and dimensions using methods described previously (8–12). Immediately prior to the preparation of cardiac tissue samples, at least six mice in each category were CO_2-asphyxiated, and the ventricle muscle was collected rapidly and rinsed in ice-cold PBS. For pathology and histological analyses, the hearts were washed extensively in ice-cold PBS and fixed immediately with ice-cold 4% paraformaldehyde in PBS. Cardiomyocytes were isolated, and intracellular Ca^{2+} measurements were performed as described previously (8–11, 13).

Protein Sample Preparation—Organellar protein fractions were extracted from pooled ventricle tissue as described previously (14, 15). Briefly ventricle tissue from four to six mice was combined and homogenized in a Dounce homogenizer in ice-cold lysis buffer (250 mM sucrose, 50 mM Tris-HCl (pH 7.4), 5 mM $MgCl_2$, 1 mM DTT, 1 mM PMSF) using a tight fitting glass pestle. The lysate was cleared of debris by tabletop centrifugation at 800 × g for 15 min. Mitochondrial and microsomal fractions were isolated from the supernatant by further centrifugation at 8000 × g and 100,000 × g, respectively, and the supernatant served as the soluble cytosolic fraction. Protein aliquots (100 μg) were precipitated, reduced, alkylated, and digested sequentially with endoproteinase Lys-C and trypsin as reported previously (15, 16)

Proteomics Analysis—Comprehensive gel-free shotgun sequencing of reduced, alkylated, and enzymatically digested protein fractions was performed essentially as described previously (15–17). Briefly the peptide mixtures were solid phase-extracted, acidified with formic acid, and loaded manually onto biphasic 100-μm-inner diameter microcapillary fused silica columns packed sequentially with strong cation exchange beads (Partisphere, Whatman, Clifton, NJ) and reverse phase resin (Zorbax Eclipse XDB-C_{18}, Agilent Technologies, Mississauga, Ontario, Canada). The columns were placed in line with a quaternary HPLC pump interfaced using electrospray ionization to an LTQ linear ion trap mass spectrometer (Thermo Finnigan, San Jose, CA). The bound peptides were eluted using a 12-step × 100-min salt/water/acetonitrile gradient (15, 16). Precursor ions (400–2000 m/z) were subjected to data-dependent, collision-induced dissociation with dynamic exclusion enabled. The resultant ~12.5 million acquired MS/MS spectra were cross-matched against a compilation of 29,051 annotated UniProt mouse (*Mus musculus*) protein sequences downloaded from the European Bioinformatics Institute on March 11, 2004 using a distributed version of the SEQUEST search algorithm (SEQUEST-PVM version 27 (revision 9) (1993); peak lists were automatically generated using the embedded ExtractMS script with default parameter settings) (18). Precursor mass tolerance was set to 3 Da (with daughter mass ion tolerance set to the default of 0), enabling fully tryptic enzyme status, single site missed cleavages, and a static chemical modification of +57 amu on cysteine (carboxyamidomethylation). The statistical probability of each primary match was assessed using the STATQUEST algorithm (15, 16). To minimize false positives, protein identifications were accepted if the candidates had a minimum of three high confidence (99%+ probability) supporting spectra that matched to at least two unique (unambiguous) peptides. To determine the FDR, we performed an empirical confidence test by searching approximately half of the spectra against a decoy database consisting of fully inverted protein sequences appended to the original native database entries. Applying the same filter criteria, the proportion of decoy (reverse) matches was found to be 0.0146% at the peptide level (50 reverse and 342,740 native peptide matches) and 0.49% at the protein level (eight reverse and 1611 native protein matches). Hence we estimated the FDR rate across the entire data set at less than 1%, which is comparable to our FDR reported previously in Kislinger *et al.* (16).

Data Normalization and Filtering—The total combined number of high confidence spectral counts per protein was summed across subcellular fractions as an estimate of relative protein abundance and possible differential expression between the R9C- and control-derived samples (16, 19). Differences in protein levels between diseased and wild-type samples recorded between the 137 different experimental runs can represent biologically relevant differences in protein expression but can also contain bias and noise. To account for spurious variance, the data were normalized. The data generated within each experiment were first separated into an equivalent number (100) of bins based on the observed spectral count value distribution. Each bin, for all the runs, was then normalized by local polynomial regression fitting (Lowess) (20) to adjust for differences in the spectral counts obtained for each individual protein in relation to the total number of overall spectra obtained for a given individual sample. The aim of this normalization technique was to reduce the inherent variability that exists between different experiments, different

spectral count abundances, and different sample complexities.

After normalizing the data, to detect proteins exhibiting differential levels between the control and diseased state, we constructed two linear models. The first modeled both the control and disease states as well as the time (8, 16, and 24 weeks) and localization (cytosol, microsome, mitochondria I, and mitochondria II) as separable parameters, whereas the second model examined only time (8, 16, and 24 weeks) and localization (cytosol, microsome, mitochondria I, and mitochondria II) as discriminate factors. The output of the two models was compared using analysis of variance with the null hypothesis being that there is no difference, and a low p value indicated substantive discrepancy between the results of the two models, implying that the disease state was a significant determinant of the observed protein levels. To identify those proteins exhibiting a significant change in relative protein abundance as a function of disease progression, we ranked the complete set of detectable proteins based on their computed p values, a subset (593) of which exhibited nominal p values <0.05. To account for multiple hypothesis testing from the above model, the p values were then subjected to FDR correction using the Benjamini-Hochberg calculation (21, 22). This generated a final subset of 40 proteins with corrected p values <0.05 for the R9C mouse model that are reported in supplemental Table 4. The proteomics data are reported as peptides identified, whether these peptides are unique to the protein, the raw total number of matched spectra, the normalized number of matched spectra, p values, and corrected p values and are sorted according to the corrected p values.

Microarray Data Set Comparisons—Microarray-based global mRNA profiling experiments were performed using the Affymetrix Mouse 430 2.0 full-genome array chips. Protein accessions were cross-mapped to the corresponding Affymetrix probe sets. Co-inertia analysis is a multivariate method that identifies trends or co-relationships in multiple data sets and was performed to explore the covariance between the proteomics and microarray data sets essentially as described previously (23). The Bayesian probabilistic assessment was performed as described previously (16, 24).

RT-PCR Analysis—Total RNA was extracted from isolated ventricular tissue using TRIzol and subjected to RT-PCR essentially as described previously (25, 26). Primer sets were designed using WebPrimer 2.0 and purchased from AGTC Corp. (Toronto, Ontario, Canada). A complete set of primer sequences is provided in supplemental Table 4.

Western Blotting—Immunoblot analyses were performed using standard SDS-PAGE chemiluminescent procedures. Blots were processed using commercially available antibodies: mouse monoclonal to HSP47 (13510, Abcam, Cambridge, MA), mouse monoclonal to periostin (14041, Abcam), rabbit polyclonal to protein-disulfide isomerase (539229, Calbiochem), mouse monoclonal to protein-disulfide isomerase (MA3-019, Affinity Bioreagents, Golden, CO), rabbit polyclonal to Filamin A (4762, Cell Signaling Technologies, Danvers, MA), rat monoclonal to IGFBP-7 (MAB2120, R&D Systems, Minneapolis, MN); rabbit polyclonal to Nogo (IMG-5346A, Imgenex/Cedarlane Laboratories, Hornby, Ontario, Canada), rabbit polyclonal to calreticulin (PA1-903, Affinity Bioreagents), mouse monoclonal to Annexin 1 (BD Biosciences), mouse monoclonal to annexin 2 (sc-9061, Santa Cruz Biotechnology, Santa Cruz, CA and A14030, BD Biosciences), rabbit polyclonal to GRP78 (PA1-014, Affinity Bioreagents), mouse monoclonal to GRP94 (MA3-016, Affinity Bioreagents), rabbit polyclonal to four and a half LIM domain (FHL1) (IMG-3374, Imgenex/Cedarlane Laboratories), mouse monoclonal to Talin-1 (TD-77, Genetex, San Antonio, TX), rabbit polyclonal to dihydropyrimidinase 3 (DPY3) (23951, Abcam), rabbit polyclonal to cofilin-1 (11062, Abcam), mouse monoclonal to vimentin (MA3–745, Affinity Bioreagents), rabbit polyclonal to cofilin-1 (11062, Abcam), rabbit polyclonal to IQGAP (sc-10792, Santa Cruz Biotechnology), rabbit polyclonal to S100-α (PA1-932, Affinity Bioreagents), mouse monoclonal to CHOP (MA1-250, Affinity Bioreagents), rabbit polyclonal to glyceraldehyde-3-phosphate dehydrogenase (PA1-968; Affinity Bioreagents), and rabbit polyclonal to UCHL1 (U5382, Sigma). Apoptosis antibodies were obtained from Cell Signaling Technology Inc.: caspase 3 (9668), caspase 9 (9504), and caspase 12 (2202).

Cytochemistry and Pathology—*In situ* DNA end labeling and hematoxylin and eosin staining were performed at the Department of Pathology, University Health Network, Toronto, Ontario, Canada. Sections were analyzed on a Leica stereomicroscope.

Tissue Samples—Human tissue and blood samples were collected according to protocols with appropriate ethics approval at Harvard/Massachusetts General Hospital and the Toronto General Hospital/University Health Network. Patients with dilated cardiomyopathy were classified as Stage III/New York Heart Association Class III according to standard criteria. Plasma samples were precleared of IgG and albumin using two cycles through Proteo-extract columns (Calbiochem) and subjected to immunoblot as described above (Larial Proteomics, Toronto, Canada). For the global proteomics profiling of the PLN-R9C human cardiac explant, the frozen ventricular tissue biopsy was homogenized in a Dounce homogenizer in solubilization buffer and fractionated essentially as outlined for mouse heart above. The cytoplasmic fraction was subjected to three separate rounds of LC-MS profiling with the spectra processed essentially as described above.

Cross-referencing On-line Data Sets—Protein predictions for secretion were made according to the on-line predication algorithm PSort II (27) and the Secreted Protein Database (28) available publicly. We also cross-referenced our highly ranked proteins to the experimentally predicted human urine proteome (29) and human plasma proteomes (30, 31).

RESULTS

Development of Dilated Cardiomyopathy in the R9C Transgenic Mouse Model—We established a survival curve for the transgenic line in which 44 mice overexpressing the R9C transgene under control of the myosin heavy chain, cardiac-specific promoter and 79 littermate controls were analyzed. The PLN-R9C mice had a median survival of only ~20 weeks with fewer than 15% persisting past 24 weeks (Fig. 1*A*). The first recorded deaths in the PLN-R9C line were observed between 12 and 16 weeks of age, whereas only one wild-type control mouse died over the entire 24-week period. For our subsequent detailed proteomics analyses (see below), 24 weeks was established as end stage human dilated cardiomyopathy due to the high mortality, 8 weeks was established as a time point representative of early stage disease prior to the first recorded mortality, and 16 weeks was established as a midpoint in disease progression. However, enlargement of both ventricle and atria was evident by 8 weeks of age in the PLN-R9C mice (Fig. 1*B*). Likewise cross-sections of the myocardium stained with hematoxylin and eosin (Fig. 1*B*) showed thinning of the ventricular wall and evidence of left ventricular dilatation in the 8-week transgenic animals with continued progression of dilatation with age. High power magnification also indicated obvious regions of fat and connective tissue infiltration and muscle degeneration in the PLN-R9C hearts even at the 8-week time point (Fig. 1*C*).

Decreased Function in Cardiomyopathy Hearts—Functional

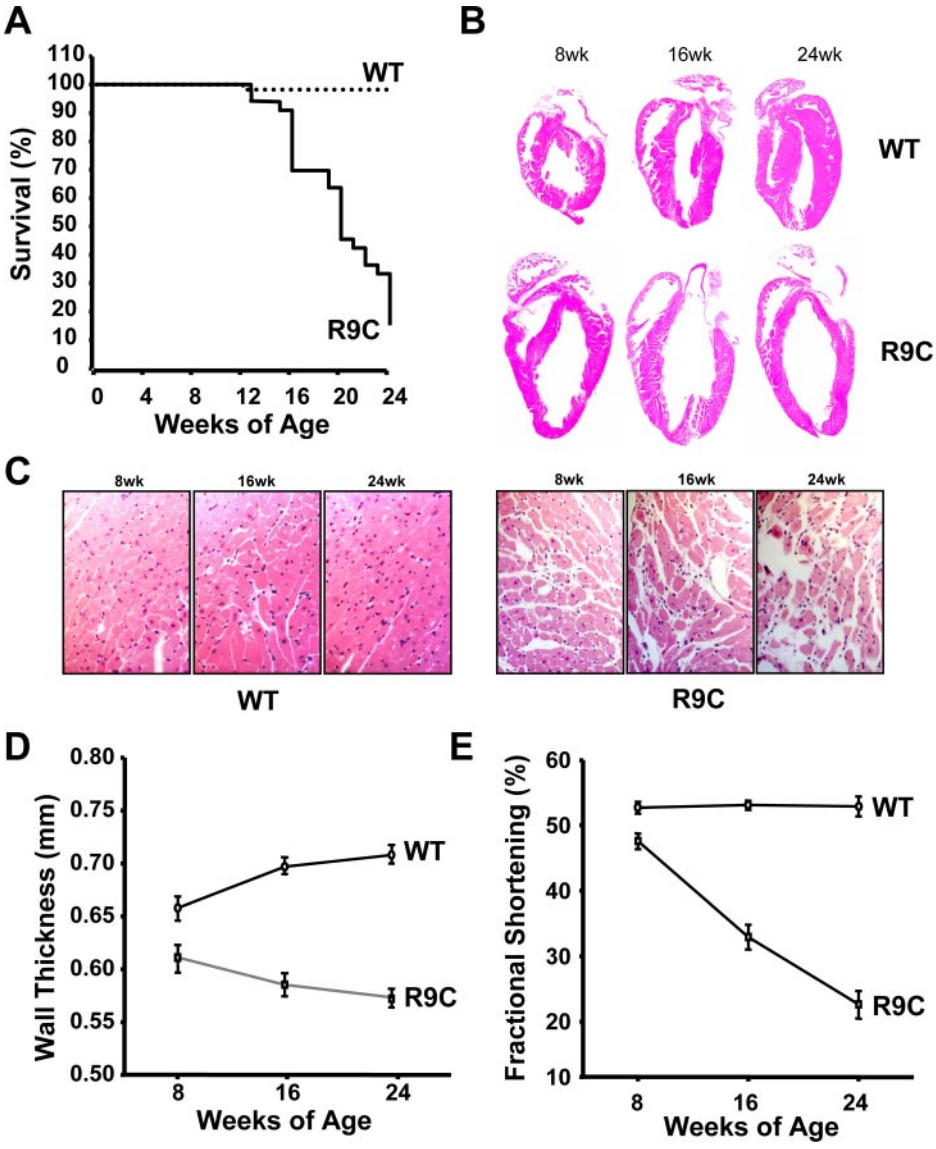

FIG. 1. **Phenotypic analyses of wild-type and R9C mice.** *A*, survival curves for wild-type mice (*WT*) ($n = 79$) and R9C mice ($n = 44$) were generated following a 24-week period. *B*, cardiac sections show significant cardiac enlargement in the R9C mice even at the earliest time point of 8 weeks of age. Prominent in the sections is the left ventricular dilatation present at 8 weeks and throughout 16 and 24 weeks of age. *C*, higher power micrographs show evidence of cardiac disease also evident from 8 weeks of age. *D*, echocardiography and measurement of anterior and posterior wall thickness in wild-type and R9C mice. *E*, cardiac shortening assessed by echocardiography. Significant functional impairment in the R9C transgenic animals begins as early as 8 weeks of age.

cardiac measurements were performed by echocardiography on individual 8-, 16, and 24-week-old male and female mice; although female mice showed identical findings, only the data obtained for male mice are provided in Fig. 1*D* and Table I. Echocardiographic measurements of the thickness of the anterior and posterior walls (Fig. 1*D*) indicated that the R9C mice had significant dilatation at 8 weeks, which progressed throughout the lifespan of these mice. However, contractility, as assessed by cardiac fractional shortening (Fig. 1*E*), was only slightly, albeit significantly, reduced by 8 weeks, whereas a far more pronounced decrease was evident by 16 weeks.

Proteomics Assessment of Progressive Heart Failure—Using the survival curves, echocardiography, and pathology as guides, we proceeded to examine the global protein complement of ventricular muscle isolated from wild-type and R9C mice at 8, 16, and 24 weeks of age to identify those proteins exhibiting altered abundance as a function of disease progression. To achieve high sensitivity and comprehensive coverage, we performed gel-free shotgun sequencing of extensive proteolytic digests of ventricular muscle protein extracts using high performance multidimensional capillary-scale liquid chromatography coupled to automated data-dependent tandem mass spectrometry (see "Experimental Procedures"). To alleviate the severe dynamic range limitations stemming from components of the highly abundant contractile apparatus (14, 15, 17), we first isolated cytosolic, mitochondrial, and microsomal protein fractions from homogenized cardiac tissue pooled from several animals using differential ultracentrifugation (nuclear fractions proved harder to separate from abundant contractile proteins and hence were excluded from this study). Each fraction was analyzed repeatedly; nine times at 8 and 16 weeks and four times at 24 weeks, to enhance overall detection sensitivity and coverage.

A total of 12,847,690 spectra were acquired and searched

TABLE I

Echocardiographic and hemodynamic parameters in wild-type and R9C mice at 8, 16, and 24 weeks in male and female mice

Values are mean ± S.E. HR, heart rate; AW and PW, anterior and posterior wall thickness (left ventricle), respectively; LVEDD and LVESD, left ventricular end diastolic and systolic dimension, respectively; FS, fractional shortening = (LVEDD − LVESD)/LVEDD × 100%; ETC, ejection time corrected for HR; VCFC, velocity of circumferential shortening corrected for HR = FS/ETC; PAVc, peak aortic velocity corrected for HR; E-wave = early filling transmitral diastolic wave; AVA, aortic velocity acceleration (PAVc/acceleration time); WT, wild type; M, male; bpm, beats/min; circ, circumferences.

	WT	R9C	WT	R9C	WT	R9C
Age (weeks)	8	8	16	16	24	24
Gender	M	M	M	M	M	M
HR (bpm)	560 ± 6	567 ± 5	569 ± 5	552 ± 15	565 ± 9	502 ± 15[a]
AW (mm)	0.66 ± 0.01	0.60 ± 0.01[a]	0.70 ± 0.01	0.58 ± 0.01[a]	0.71 ± 0.01	0.57 ± 0.01[a]
PW (mm)	0.66 ± 0.01	0.61 ± 0.01[a]	0.70 ± 0.01	0.59 ± 0.01[a]	0.71 ± 0.01	0.57 ± 0.01[a]
LVEDD (mm)	3.82 ± 0.05	4.01 ± 0.03[a]	3.92 ± 0.07	5.01 ± 0.06[a]	3.99 ± 0.05	5.48 ± 0.08[a]
LVESD (mm)	1.82 ± 0.05	2.13 ± 0.04[a]	1.84 ± 0.06	3.36 ± 0.09[a]	1.89 ± 0.03	4.23 ± 0.09[a]
FS (%)	52.7 ± 0.9	47.6 ± 1.2[a]	53.1 ± 0.7	32.9 ± 1.9[a]	52.9 ± 1.5	22.6 ± 2.1[a]
VCFc (circ/s)	10.5 ± 0.2	9.1 ± 0.2[a]	10.5 ± 0.1	7.0 ± 0.5[a]	10.9 ± 0.3	5.1 ± 0.5[a]
PAVc (cm/s)	102.4 ± 2.4	97.8 ± 2.6	110.1 ± 3.7	85.3 ± 3.2[a]	111.3 ± 2.9	73.6 ± 3.1[a]
AVA (m/s^2)	65.7 ± 1.3	60.6 ± 1.6	66 ± 3.2	47.9 ± 2.5[a]	67.1 ± 3.1	40 ± 2.2[a]
Samples (*n*)	6	9	6	9	5	5

[a] $p < 0.05$ compared with WT.

against a reference mouse protein sequence database. Candidate matches were subjected to two rounds of stringent filtering (see "Experimental Procedures"). First, we used a rigorous statistical model (14) to assign confidence scores to individual database matches, accepting only those candidate identifications supported by two or more high scoring (*p* value <0.01) peptides. Second, we eliminated redundancy by accepting only those proteins supported by two or more unambiguous (*i.e.* unique) peptide sequences (16). This parsing resulted in a final set of 6190 high confidence protein identifications (supplemental Table 1); an additional set of 1072 candidates, tentatively identified with multiple high scoring spectra mapping to either only a single peptide ($n = 828$) or, more ambiguously, to peptides shared among a cluster of closely related proteins ($n = 244$), were removed from further consideration but are reported for completeness in supplemental Table 2. All relevant spectral information for all high confidence identifications, including the protein name, primary accession, description, search scores, and associated statistical information as well as links to the supporting MS/MS evidence, is freely available on a dedicated Web server with a searchable interface.[2]

Large Scale Differential Expression throughout the Time Course—Quantitative differences in relative protein levels between the healthy and diseased mice were estimated on the basis of the measured ratio of the total number of accumulated high confidence spectra obtained for each protein in the R9C *versus* control fractions (Fig. 2*A*, *inset*). To minimize spurious variance, the repeat experimental data sets were first normalized using a global scaling parameter and then integrated prior to comparison (Fig. 2*A*). We then applied a linear regression model (see "Experimental Procedures") to identify those 593 proteins that exhibited statistically significant (*p* value <0.05) differential abundance in the diseased state (supplemental Table 3). A background average false discovery rate of <200 proteins was estimated based on permutation of the experimental labels (Fig. 2*B*). Following the application of a Benjamini-Hochberg calculation for FDR correction, adjusted *p* values (*i.e. q* values) were obtained; a subset of 40 top ranked proteins with $q < 0.05$ are shown in supplemental Table 4.

A heat map schematic of the perturbed protein patterns, sorted by statistical rank, is provided in Fig. 2*C*. Within this list of candidates are proteins previously linked functionally to cardiomyopathies, including atrial natriuretic factor (ANF) and angiotensin-converting enzyme (ACE), which are archetypal components of the adaptive homeostatic response to hypertension, as well as cytoskeletal factors linked to cardiac remodeling, such as actins, myosins, annexins 1 and 2, spectrin, and desmin (32–35). (The classic biomarker of HF, BNP, was tentatively detected as up-regulated in the failing heart (a total of 10 spectra in R9C *versus* only one for wild type), but as it was identified with only one unique peptide it was formally excluded along with 827 other putative proteins identified with limited spectral support (see supplemental Table 2).) Detection of these well established proteins validates the overall effectiveness of the proteomics screening, data processing, and statistical filtering procedures.

Affected Protein Categories in Maladapted Cardiac Tissue—Hierarchical clustering of the high confidence candidates (Fig. 2*C*, *top panel*) revealed elevated expression of a substantial fraction (467) of proteins at 8 and/or 16 weeks, whereas another 70 showed consistent up-regulation throughout disease progression (elevated levels in all three time points). Conversely 126 proteins showed reduced overall abundance (Fig. 2*C*, *bottom panel*).

[2] A. Emili, personal communication.

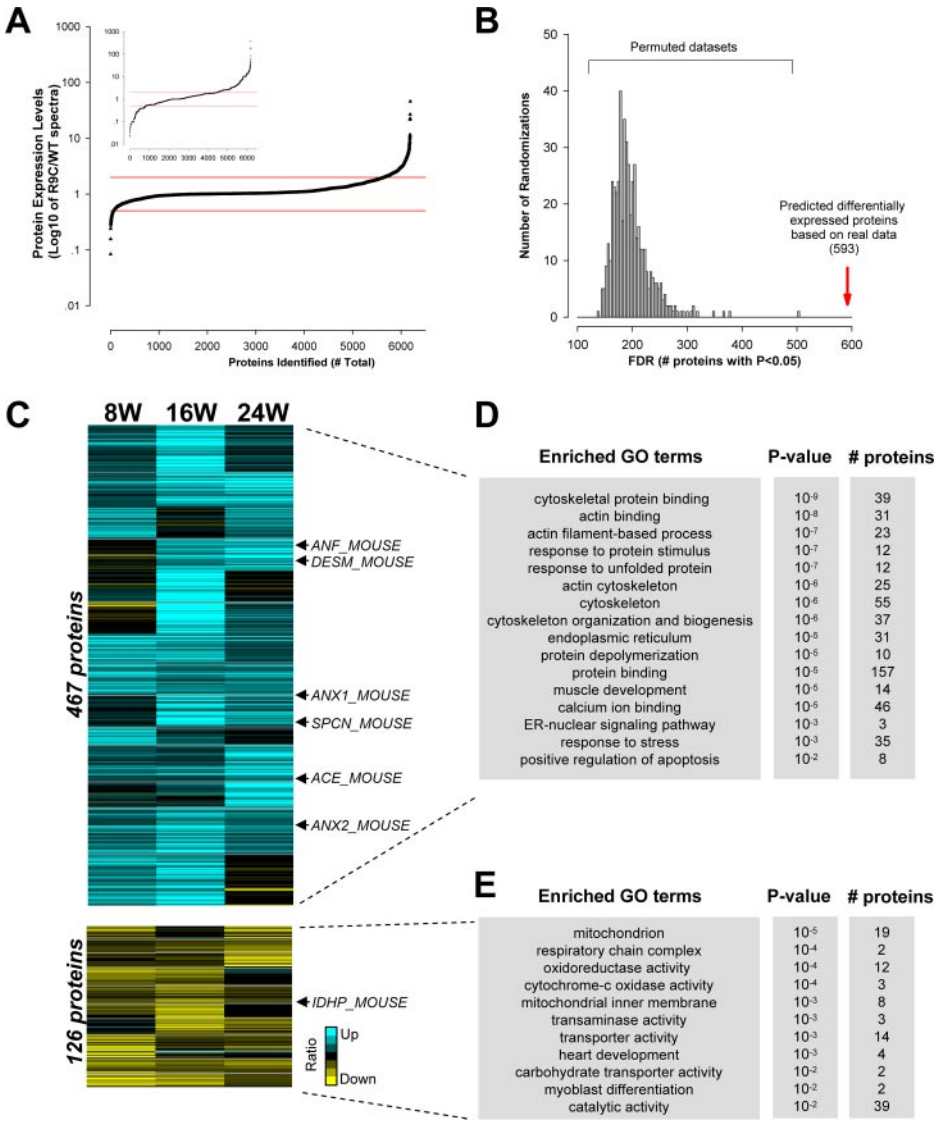

FIG. 2. **Gel-free shotgun analyses of cardiac ventricular samples.** *A*, proteins were identified, and expression levels were semiquantified using spectral counts at all of the three time points. Abundance levels of proteins are shown in a log scale plot. The profiles were subjected to normalization to address variation in mass spectrometry acquisition. *Inset*, unfiltered data. *Red lines* represent a 1-fold difference from controls. *B*, calculation of the false discovery rate. *C*, statistical modeling resulted in the identification of 593 proteins found to be significantly different between wild-type (*WT*) and R9C hearts. The expression profiles of these proteins were plotted in log scale and hierarchically clustered. Shown are 467 proteins that were up-regulated in disease and 126 proteins that were down-regulated. Proteins previously identified to be up-regulated in dilated cardiomyopathy are marked at the *right*, including ANF, DESM, ANX1, SPCN, ACE, ANX2, and IDHP (isocitrate dehydrogenase). *Blue*, up-regulated expression; *yellow*, down-regulated expression. *D* and *E*, significantly enriched GO terms within the 593-protein data set. Enriched GO and phenotype ontology terms are listed together with *p* values and the number of proteins sorted in each category. *D* represents GO categories significantly over-represented in R9C, whereas *E* represents GO categories found to be under-represented. *W*, weeks.

Statistically significant over-representation among select GO categories was detected among annotated proteins in both the up- or down-regulated sets (Fig. 2, *D* and *E*). Functions exhibiting marked increases in the PLN-R9C mice included cytoskeletal and calcium ion-binding proteins, ER, chaperone-mediated protein folding, the ER stress response, and activation of apoptosis. There were also marked decreases in mitochondrial proteins associated with fatty acid oxidation, consistent with a shift to glucose metabolism in the diseased state. These changes are consistent with a major reorganization of the cardiomyocyte cytoskeleton as a maladaptive attempt to compensate for decreased cardiac function (36, 37). These results, viewed together with the echocardiography and histology data, indicate that, even by 8 weeks of age, R9C cardiac ventricular muscle is subject to considerable biochemical stresses that cannot be fully compensated for, resulting in the initial stages of HF.

Comparison of Proteomics Data with mRNA Patterns—The reliability of our proteomic candidates was assessed by comparison with gene expression levels as recorded in parallel mRNA measurements using high density DNA microarrays (see "Experimental Procedures") (23). Co-inertia analysis (CIA), an unbiased multivariate method for examining general trends (co-relationships) among disparate data sets, indicated excellent correspondence between the global protein and mRNA profiles (Fig. 3*A*). A further indication of overall agreement in the cognate patterns for the 593 statistically relevant proteins was evident by hierarchical clustering (Fig. 3*B*), particularly among the seemingly higher abundance gene products. This heat map also highlights the extensive proteomic changes observed at the early and midstage time points (8 and 16 weeks), indicating substantial protein remodeling and biochemical changes that are not evident by microarray analyses to the same extent. However, cytoskeletal remodeling, ER stress responses, and Ca^{2+} signaling responses (Fig. 2, *C* and *D*) are consistent with the phenotypic changes observed

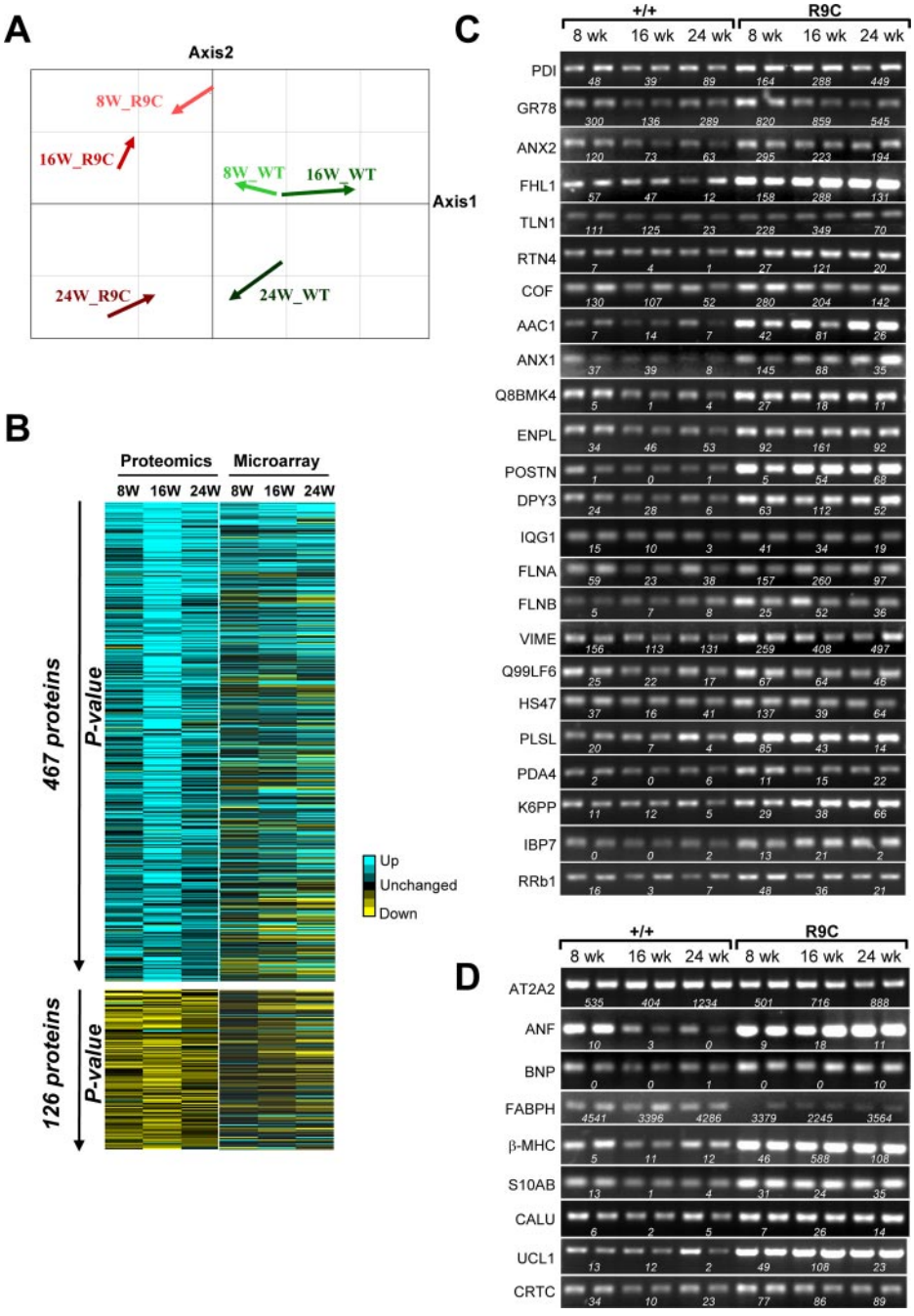

FIG. 3. **Comparison of the 593 candidates identified by MudPIT with parallel mRNA microarray analyses.** Microarray experiments were performed on ventricular tissues using Affymetrix chips. CIA plots were performed on the microarray and proteomics data and are shown in *A*. The six samples are plotted in the first two dimensions of a CIA. Each *arrow* shows the location of the sample in gene space (*base* of the *arrow*) and protein space (*arrow tip*). *Axis2* clearly separates the PLN-R9C and wild-type (*WT*) samples, and the *length* of the *arrow* in each case is related to the divergence between the two data sets. *B*, a protein cluster, based on descending *p* values of 593 proteins, is opposed to a cluster of cognate mRNA data. The correlation between the results of the two experimental platforms is evident. *C*, RT-PCR analysis of 24 of the top proteins shows strong correlation with the proteomics data set. The proteomics spectral counts are shown in the *inset* on each agarose gel. *D*, additional candidates chosen at random were subjected to RT-PCR. *W*, weeks.

at these same time points, namely increased mortality and decreased cardiac function (Fig. 1).

Because standard metrics (*e.g.* Pearson or Spearman) lack a suitable noise model or principled confidence measure to assign statistical significance, we applied a Bayesian probabilistic approach (16) (see "Experimental Procedures") to measure the correlation directly. We used a Bernoulli switch variable to explain the mRNA abundance as a linear function of the recorded protein spectral counts or a learned background distribution. Spurious variance in the protein and mRNA levels was modeled using Gaussian and Poisson distributions, respectively, and a confidence score was calculated by permutation testing. Of the 593 perturbed proteins, only 16 were deemed to be significantly non-correlated outliers (supplemental Table 5), none of which were top ranked proteins. The biological significance of these outliers is uncertain but could reflect post-transcriptional regulation.

Validation of Proteomics Data—We attempted further validation of the differential abundance of top ranked gene products that showed the most significant differential increase in the disease state using semiquantitative RT-PCR assays. As expected, we observed marked up-regulation of correspond-

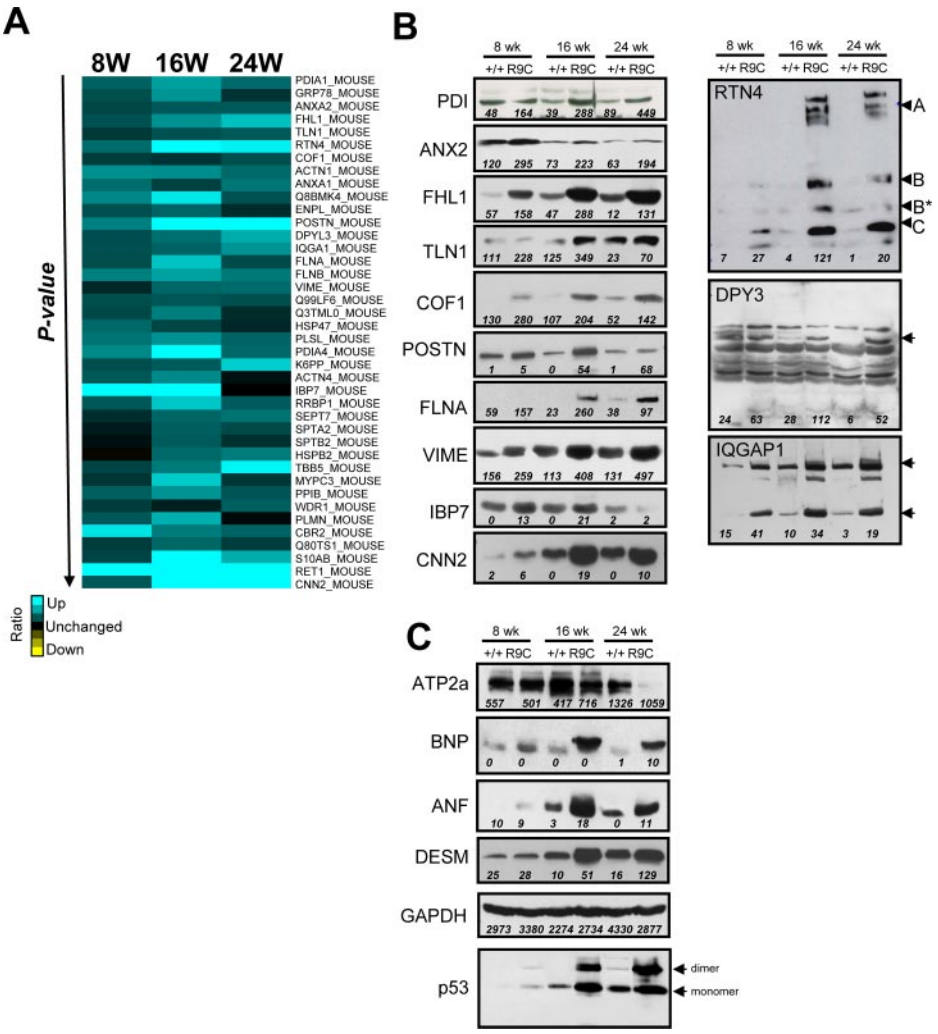

FIG. 4. **Immunoblot validation of proteomics data.** *A*, hierarchical clusters of the 40 highest ranked proteins, which survived the false discovery Benjamini-Hochberg correction. Shown are the ratios of spectral counts in the R9C:wild type at 8, 16, and 24 weeks of age. *B*, immunoblot analyses of a number of the top 40 proteins were performed when commercial antibodies were available, and the results are shown. Blots with multiple bands are shown in the *right panel*. *Arrows* indicate protein bands of the expected molecular weight. For RTN4, several isoforms exists and were detected in our experiments. *C*, additional proteins were examined including ATP2a, BNP, ANF, p53, and DESM. *W*, weeks; *GAPDH*, glyceraldehyde-3-phosphate dehydrogenase.

ing transcripts for virtually all of the 24 proteins examined (Fig. 3*C*) in PLN-R9C mice relative to control, consistent with the predicted proteomic profiles. There was also excellent accord between the measured protein abundance and mRNA abundance for another ~75 gene products selected on the basis of general applicability to cardiac function or disease (including AT2A2, ANF, BNP, FABHP, and β-MHC) or chosen at random (S10AB, CALU, UCL1, and CRTC); several of these are shown in Fig. 3*D* (see supplemental Fig. 1 for additional information).

Fig. 4*A* shows a clustergram heat map, based on corrected *p* value, of the 40 proteins that passed the most demanding FDR assessment. In general, these proteins were among the most abundantly up-regulated factors induced in R9C over the 24-week period.

As one final, alternate, and arguably more stringent measure to confirm the reliability of our proteomics predictions, we performed immunoblot analyses to examine protein levels for 23 of these candidates for which commercial antibodies were available. Again fully consistent with the proteomic profiles, the microarray data, and RT-PCR experiments, we confirmed significantly elevated levels for virtually all of the top ranked proteins in the diseased state (Fig. 4*B*), including PDI, ANX2, FHL1, TLN1, COF1, POSTN, FLNA, VIME, IBP7, CNN2, RTN4, DPY3, and IQGAP1. As additional controls (Fig. 4*C*), we examined the protein levels of ATP2a, BNP, ANF, DESM, and p53 by Western blotting because their expression has been reported previously to change in dilated cardiomyopathy (32–35, 38). Consistent with expectation and our own proteomics results, BNP, ANF, DESM, and p53 were all significantly up-regulated in the R9C mice, whereas ATP2a was down-regulated as noted before. As a loading control, glyceraldehyde-3-phosphate dehydrogenase levels were also measured and were unaffected.

Noticeable differences in protein levels were detectable between the various time points. Given that we were able to verify the changes in expression detected by proteomics profiling through comparable changes detected by immunoblotting for most proteins examined, it is likely that the large phenotypic changes we observed (Fig. 1) indicating substantial compensatory and remodeling pathways in the 16-week R9C mouse and severe cardiac pathology leading to death at 24 weeks correlate functionally with these proteomic variations.

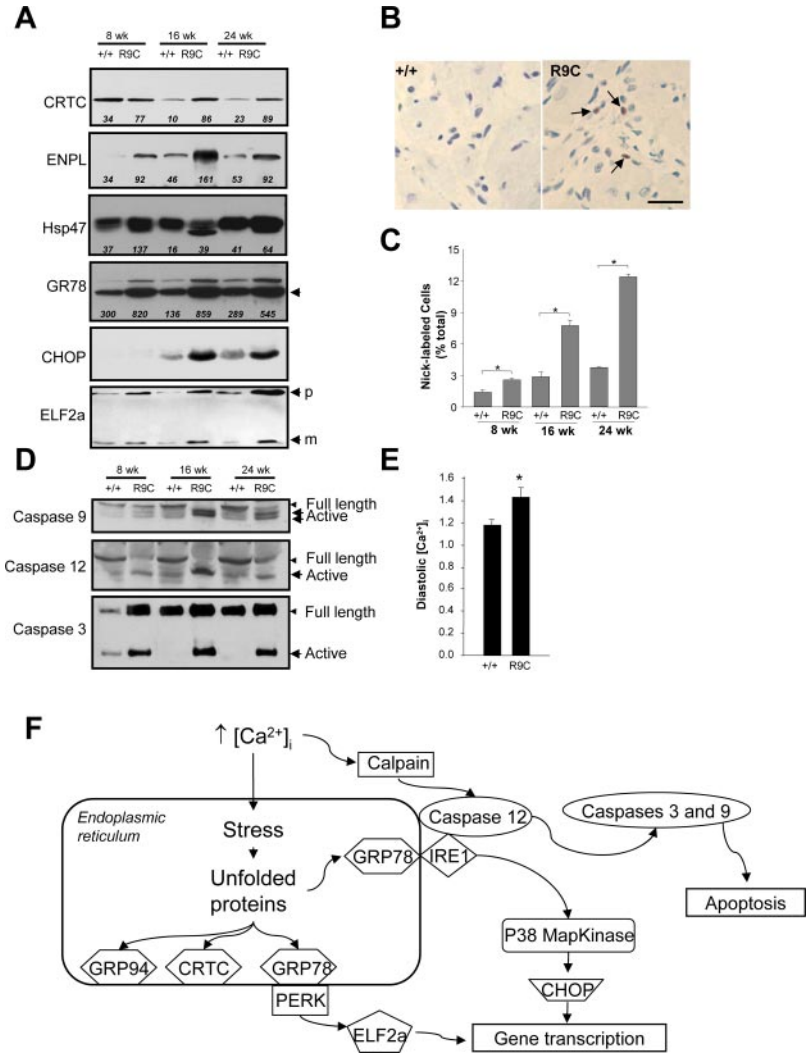

FIG. 5. **Cellular stress responses in dilated cardiomyopathy.** Enriched GO terms and proteomic candidates indicated significant activation of ER stress in the R9C heart. *A*, immunoblot analysis of several ER stress proteins shows up-regulation of CRTC, GRP94 (ENPL), HSP47, GRP78, CHOP, and ELF2. *B* and *C*, nick labeling of cryostat sections of wild-type and R9C hearts shows the activation of apoptosis in R9C over a period of 24 weeks. *D*, levels of cleaved and activated caspases 3, 9, and 12 also increase in R9C over a period of 24 weeks. *E*, diastolic calcium levels measured in isolated cardiomyocytes were increased significantly in R9C. *F*, schematic diagram of Ca^{2+}-induced ER stress responses. *, $p < 0.05$, significantly different from wild type, Student's *t* test. Data are shown as mean ± S.E.

Pathways Activated in Heart Failure—The results of our proteomics screens are consistent with the hypothesis that dysregulation of Ca^{2+} cycling in the PLN-R9C myocytes leads to activation of ER stress pathways and apoptotic cell death. To verify whether such responses were indeed activated, we examined the status of key regulators known to mediate the ER stress responses (39), including CRTC, ENPL, HSP47, GRP78, CHOP, and ELF2a (Fig. 5*A*). In all cases, we verified significant up-regulation of these proteins in R9C mice, even at the earliest time point, consistent with both our proteomics predictions and with the results of two recent reports examining different mouse models of cardiac dysfunction leading to HF (40, 41).

ER stress is known to initiate apoptosis (39), and significant activation of apoptosis was detectable during progression to dilated cardiomyopathy in the R9C ventricle by DNA end labeling (Fig. 5, *B* and *C*). Signaling cascades involved in apoptosis linked by ER stress are known to converge on several key caspases, particularly caspases 3, 9, and 12 (see Refs. 39 and 42). Immunoblotting for caspases 3, 9, and 12 showed evidence of substantial activation of all three proteases by 8 weeks in the R9C ventricle alone (Fig. 5*D*).

Because the PLN-R9C mutation is likely to perturb cytosolic Ca^{2+} levels and because altered Ca^{2+} may contribute to the induction of apoptosis and myocyte remodeling (5, 6, 37, 43, 44) we measured the intracellular Ca^{2+} concentration in isolated cardiomyocytes obtained from the R9C mice *versus* wild-type controls. Cardiomyocytes were isolated from 6–8-week-old animals because cells isolated from older animals generally fail to give reproducible recordings. Even at this early time point, resting intracellular Ca^{2+} levels were found to be increased significantly in the R9C cardiomyocytes (Fig. 5*E*), providing a rationale for the ER stress response as a result of dysregulation of Ca^{2+} cycling, which in turn induces apoptosis and remodeling of the R9C cardiac muscle. A model of the potential interactions between elevated Ca^{2+} and ER stress pathways, incorporating key proteins activated in R9C, including calpain; caspases 3, 9, and 12; GRP78; GRP94; CRTC; ELF2a; and CHOP, is presented in Fig. 5*F*.

Detectable Expression in a Human Cardiac Explant—The

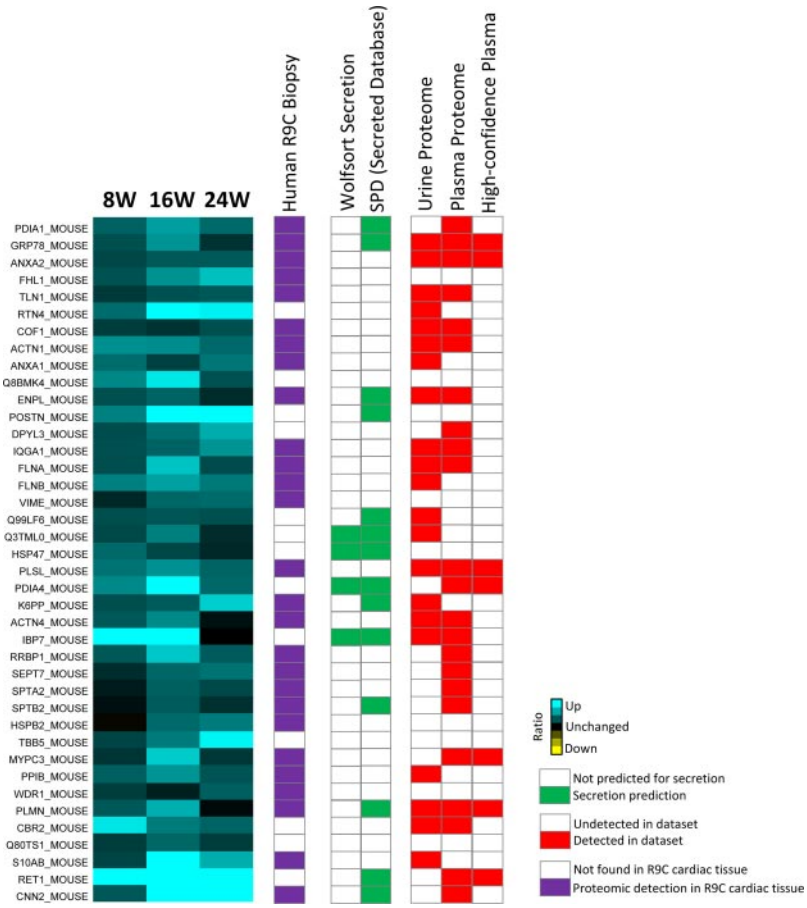

FIG. 6. **Mapping of the 40 highest ranked candidates against a human R9C ventricular explant and on-line data sets.** The 40 most differentially up-regulated proteins detected in R9C mouse ventricular tissues were compared against protein identifications in the cytosolic compartment isolated from a human R9C cardiac explant. The presence or absence of the human homologues of the proteins is indicated. The two *panels* with *green boxes* indicate proteins predicted to be secreted using on-line prediction algorithms. In the first and second of the *panels* with *red boxes*, proteins found in the human urine and plasma proteome are indicated. *W*, weeks.

availability of cardiac tissue from a human R9C proband made it possible to investigate the presence of the top 40 mouse ventricular proteins in a proteomics screen of the analogous corresponding human disease (Fig. 6). Because control healthy samples were not available to perform an exhaustive comparison, we did not attempt to quantify the expression levels but rather assessed which, if any, orthologues of the top ranked 40 candidates were similarly detectable in the human explant. Encouragingly all but 13 were identified in the human pathological sample. (The fact that we did not detect all might reflect, in part, incomplete cross-mapping or limited annotations as opposed to a true absence of the corresponding proteins.)

Secretion and Serum Elaboration in Mouse and Man—We explored the possibility that some of the top ranked candidates might be developed as biomarkers of dilated cardiomyopathy, including early stage disease. First we determined which proteins either possess potential secretory properties or have been reported as being present in the human urine (45) and plasma (30) proteomes. Using the Wolfsort PII prediction (27) and information from the Secreted Protein Database (28), we found that PDIA1, GRP78, ENPL, POSTN, Q99LF6, Q3TML0, HSP47, PDIA4, K6PP, IBP7, SPTB2, PLMN, RET1, and CNN2 are all potentially secreted proteins. Of particular interest, 30 of the candidates were detected previously in human urine, human plasma, or both. Plasma proteins include PDIA1, GRP78, TLN1, COF1, ACTN1, ENPL, DPY3, IQGAP1, FLNA, PLSL, ACTN4, IBP7, RRBP1, SEPT7, SPTA, SPTB, MYPC3, PLMN, CBR2, RET1, and CNN2.

Monitoring the levels of these candidates in the systemic circulation could potentially serve as a useful surrogate indicator of cardiac integrity. First we assessed the levels of RTN4, HSP47, IBP7, ENPL, POST, and IQGAP1 in mouse plasma obtained from wild-type and R9C transgenic animals (Fig. 7, *A* and *B*) because commercial antibodies were available and we had determined that many of these antibodies could be assayed in plasma experiments due to reasonably low nonspecific background staining (results not shown). Although many of the antibodies including, for example, anti-COF1, -RET1, and -CNN2, failed to show any specific signals at the correct molecular weights, our experiments were strikingly successful in that six of the assayable proteins were both detectable in plasma and showed increased resting levels in the R9C samples (Fig. 7, *A* and *B*). For POST and IQGAP1, appropriate bands were present only in the R9C-derived serum samples.

To address the clinical potential of candidates validated in mouse plasma, we likewise examined human plasma with the available reagents. First the cardiac explant from the R9C patient was screened with the antibodies to determine cross-reactivity between species (Fig. 8*A*). Antibodies against IQ-

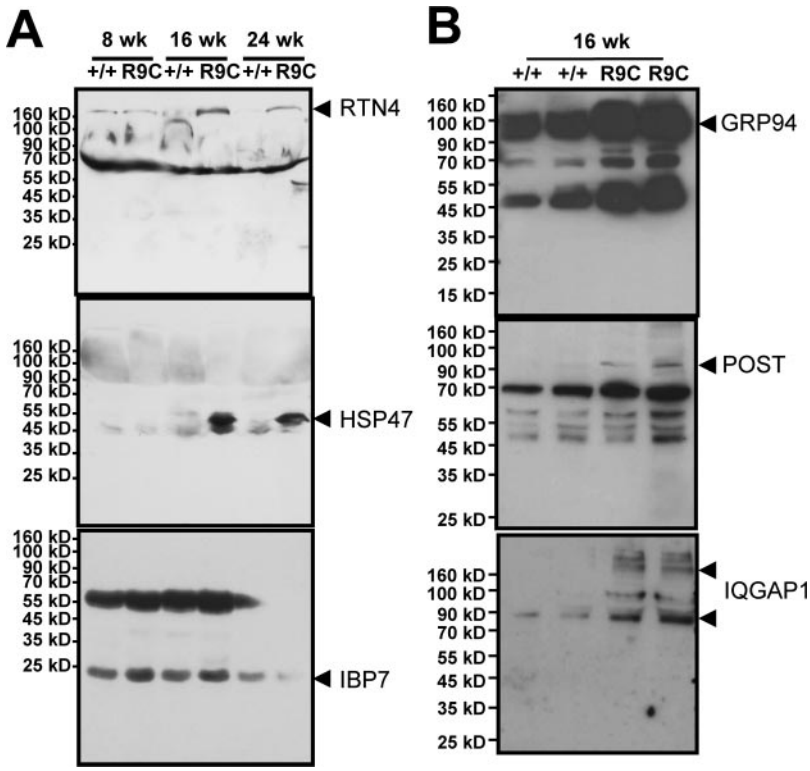

FIG. 7. **Identification of potential biomarkers in mouse plasma.** Mouse plasma was isolated from multiple animals, pooled, and subjected to one IgG depletion column followed by immunoblotting using antibodies against RTN4, HSP47, and IBP7 at 8, 16, and 24 weeks (*A*) and GRP94, POST, and IQGAP1 at 16 weeks only (*B*). All six of these proteins are elevated significantly in R9C plasma samples. Experiments using CNN2, RET1, and PDI failed to show interpretable results.

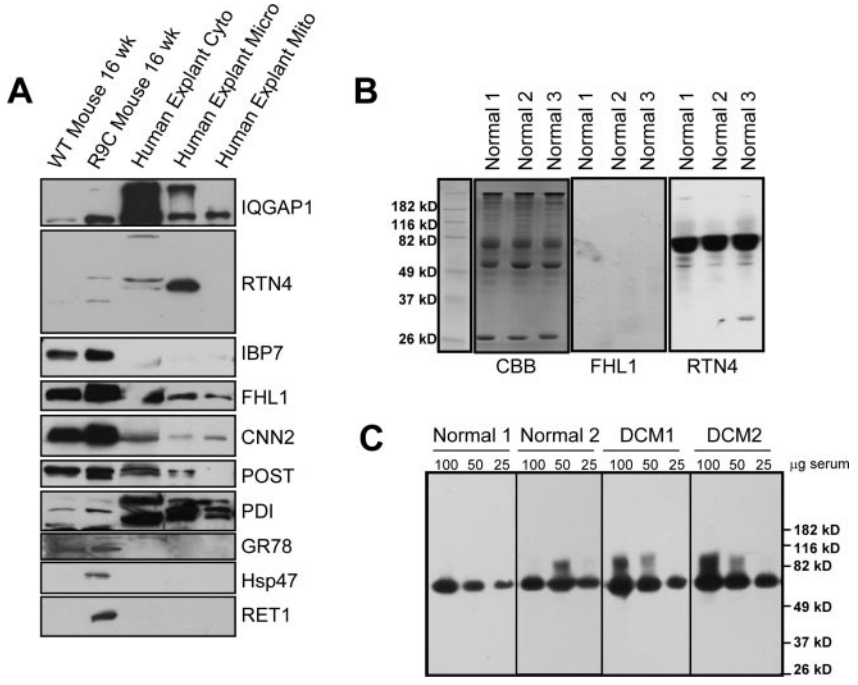

FIG. 8. **Identification of potential biomarkers in human tissue and plasma.** *A*, to determine the cross-reactivity of antibodies between mouse and human proteins, immunoblots were performed using homogenates from 16-week-old R9C mouse ventricles and different fractions from ventricular tissue from the R9C patient explant. For IQGAP1, IBP7, FHL1, and POST, single protein bands of appropriate sizes were detected. For RTN4, multiple appropriate bands were visualized with dominance of the RTN4-C isoform. RET1, GRP78, and HSP47 failed to show any signal in human tissues. *B* and *C*, human plasma samples were isolated, cleared through two sequential IgG depletion columns, and subjected to immunoblotting using the human-compatible antibodies. *C*, RTN4 was clearly visible in healthy patient plasma and showed a significant elevation in blood samples taken from two dilated cardiomyopathic (*DCM*) patients (Stage III, New York Heart Association Class III). IBP7, FHL1, and POST all failed to show any signal under any condition. *WT*, wild type; *Cyto*, cytosolic; *Micro*, microsomal; *Mito*, mitochondrial; CBB, Coomassie Brilliant Blue.

GAP1, RTN4, IBP7, FHL1, CNN2, POST, and PDI cross-reacted with the human variant, whereas anti-RET1, -GRP78, and -HSP47 did not.

Next we screened human blood samples from healthy patients to determine whether basal amounts of these factors were present in plasma under normal conditions (Fig. 8*B*). Anti-RTN4 detected a strong band at ~70 kDa, whereas bands of ~50 and 55 kDa presumably represent additional RTN variants. In contrast, IBP7, POST, and FHL1 all failed to show any signals in repeated experiments (results not shown).

In our final set of experiments, we compared the levels of RTN4 in blood samples obtained from healthy and dilated cardiomyopathic patients (Stage III/New York Heart Association Class III) (Fig. 8*C*). In these studies, RTN4 was detected in a load-dependent signal. Significantly higher levels were found in the patient cohort as compared with the healthy controls. Although limited in scope, these data motivate further evaluation of RTN4 in an expanded population cohort setting.

DISCUSSION

In this study, we performed a large scale proteomics survey of mouse cardiac disease using a rigorous comparative profiling strategy based on a relatively unbiased and sensitive method of protein detection that revealed temporal patterns of differential protein expression (14, 46, 47). This study provides a detailed molecular survey of global proteome changes linked to progressive dilated cardiomyopathy and a framework for investigating the pathways, components, and mechanisms associated with disease action. Our data implicate Ca^{2+} mishandling and subsequent ER stress and apoptotic signaling as major activated cascades, shedding light on intracellular responses that may be exploited as therapeutic targets for treating cardiomyopathy and HF. This study builds on existing targeted studies that have examined tissue- and species-specific mammalian proteomes (16, 46, 48–52) and extends information gathered using genome-wide screens of heart failure (53–55).

Relation to Proteomics Studies in Cardiac Tissue—Previous proteomics studies using two-dimensional gel analyses have identified up to ~500 proteins in cardiac muscle with ~40 elevated in cardiac hypertrophy or cardiac dilation (15, 56–62). We cross-mapped our complete R9C protein data set onto these previously identified proteins (supplemental Table 8). Roughly one-third of the previous candidates showed consistent significant changes in our study, and one-third showed some discordance between studies (the remaining third could not be unambiguously cross-referenced). Presumably the basis for at least part of the discrepancies can be attributed to differences in proteomics detection methods, differences in the animal models assessed, and fundamental differences in the disease etiologies.

In a previous study of a mouse model of mild cardiac hypertrophy (63), we used gel-free shotgun screening to monitor the presence of 782 proteins in a microsomal fraction isolated from the cardiac ventricle. We found that 81 proteins were differentially expressed in the hypertrophic state as compared with a control group. In nearly all of the proteomics studies to date, HF has been associated with significant overrepresentation of proteins in select functional categories (*i.e.* GO terms). These include reduced mitochondrial function, disruption of energy production, and the loss of cardiac structural integrity involving significant cellular matrix and cytoskeleton remodeling (5, 6, 37, 43, 44).

Elucidation of Cellular Mechanisms in Cardiac Dilated Heart Failure—Using a stringent statistical methodology, 593 of the 6190 proteins identified in our current study displayed significantly different levels between the wild-type and R9C hearts. (Another ~1000 proteins were tentatively identified, albeit with less confidence, primarily as a result of lower spectral counts.) The identification of proteins comprising the altered profiles allowed us to interrogate more carefully the mechanisms underlying the progression of cardiac disease at least for the R9C mouse.

These proteomic changes, when analyzed for functional enrichment in GO terms, largely confirmed previous studies highlighting changes in the organization of the cytoskeleton and contractile apparatus together with systematic perturbations of energy metabolism. Other proteins and original categories found to be up-regulated in the R9C mouse include *protein degradation and ubiquitination*, *protein folding and processing*, *proteins involved in ER stress responses*, *activation of apoptosis*, *cellular metabolism*, and *Ca^{2+} ion binding*. These processes are consistent with previous knowledge of the events in dilated cardiomyopathy (5, 6, 38, 40, 64, 65) and are compatible with the proposed primary mechanism of the R9C defect (7), namely a perturbation of intracellular Ca^{2+} regulation at the level of the ER.

Concerning the ER stress response, it is clear that the ER is a central organelle responsible for protein synthesis, folding, and cellular trafficking of membrane-associated proteins. In heart, however, it is also the major intracellular Ca^{2+} storage compartment and, as such, is central to regulating intracellular Ca^{2+} levels and the contraction cycle. Perturbations of intracellular Ca^{2+} can lead to Ca^{2+} overload in the ER and protein misfolding, resulting in ER stress, a molecular pathway implicated in a wide range of pathophysiological states (64, 66). The ER stress response is characterized by increased chaperone protein expression, increased translation, and increased proteasome activation leading to protein degradation (64). Prolonged ER stress is known to induce apoptosis via activation of cellular caspases and transcription cascades involving CHOP, a key protein involved in transcriptional responses to cellular stress (64). In this study, we confirmed the activation of ER stress responses and key elements involved. Future studies aimed at addressing the relative importance of the apoptotic response in cardiac failure should resolve this important issue.

The role of other pathways involved in the progression of dilated cardiomyopathy remains to be clearly elucidated. For instance, the perturbations surrounding the significant elevation of proteins involved in cellular differentiation such as RTN4 (67), growth factors such as IGFBP7, and cytoskeletal proteins such as FHL1, CNN2 (68), and COF1 (69) and their relevance to HF remain unclear. A more detailed investigation into the functional changes preceding HF in the R9C mouse will be fruitful in elucidating novel post-transcriptional regulatory mechanisms affected in the disease. Furthermore the examination of additional mouse models of cardiac disease including other models of cardiac dilatation and pathological hypertrophy will undoubtedly reveal whether the protein perturbations seen here are common features of cardiac disease converging to HF or are restricted to the emergence of dilated cardiomyopathy, which is the hallmark of the R9C transgenic mouse.

Convergence between the Microarray and Proteomics Data—Our comparative analyses of both our proteomics and microarray data sets revealed high convergence between the top 593 proteins. Using similar correlation coefficient analyses as described previously (16), we determined that only 16 of the 593 proteins showed significantly divergent or "outlier" patterns following permutation testing. These findings are somewhat different from our previous large scale study examining proteomic and transcript levels across tissues where we observed that 503 of 1758 (~28%) protein expression profiles were different from transcript analyses (16). The differences in percent outliers likely results from the fact that in this study we focused on proteins determined to be differentially expressed, and not simply present in cardiac muscle, and that we used time course analysis to identify those gene products with consistently perturbed trajectories. Our findings are consistent with the process of cardiac dilatation as a gradual chronic condition, whereas changes in mRNA and protein expression would be expected to correlate well over the extended period (8 weeks) of analysis.

This study also highlights the potential of tissue proteomics profiling for identifying novel indicators of cardiac dysfunction. For instance, RTN4 was detected as a protein significantly overexpressed in R9C mouse ventricular muscle even from the earliest time point. Similar increases were confirmed by RT-PCR, microarray, and immunoblot experiments. Of particular interest, RTN4 was also found to be present in mouse and human plasma with plasma levels substantially elevated in both the diseased mice and in dilated cardiomyopathic patients. Other potential marker candidates, including GRP78, RET1, and POST, were studied in a similar context but were undetectable in human plasma with available antibodies/reagents. Nevertheless a notably enhanced signal for POST was confirmed in cardiomyopathic mouse plasma, and POST has been implicated as a marker of alternate disease states, such as cancer (70, 71). It is clear that the success or failure of such pilot studies, and ultimately a translation from mouse experimentation to human screening, is highly dependent upon excellent quality reagents available to the research community together with optimization of detection methods. It is hoped that, as newer antibodies, reagents, and tools become more widely available, we will be able to test some of the other top ranked candidates as markers of early stage disease.

In summary, we report substantial proteomic coverage of healthy and diseased cardiac muscle during the progression to dilated cardiac heart failure. Our results provide mechanistic insight into the process of disease progression and provide a demonstration of a proof of principle for utilizing tissue profiling to find informative markers of functional perturbation.

Acknowledgments—We thank Dr. Benoit Bruneau for assistance with whole-mount microscopy and Vijay Khanna, Wenping Li, and Eva Cuckerman for technical assistance. We thank Sarah Joe, Sadhna Phanse, and Erum Khan in the creation of the public website.

* This work was supported in part by the Canadian Institute for Health Research (CIHR) (to D. H. M., P. H. B., P. H. L., and A. E.), Genome Canada and Ontario Genomics Institute (to D. H. M., P. P. L., A. O. G., and A. E.), the Muscular Dystrophy Association U. S. A. (to A. O. G.), the Heart and Stroke Foundation of Ontario (to D. H. M. #T5042, P. P. L., and A. O. G. #NA5884), and the Natural Sciences and Engineering Council of Canada (to A. E.). Fellowship support was from the Heart and Stroke Foundation of Canada (to A. O. G. and M. G. T.), CIHR (to G. Y. O.), and the Tailored Advanced Collaborative Training in Cardiovascular Science Fellowship Program (to G. Y. O. and M. G. T.). The costs of publication of this article were defrayed in part by the payment of page charges. This article must therefore be hereby marked "*advertisement*" in accordance with 18 U.S.C. Section 1734 solely to indicate this fact.

[S] The on-line version of this article (available at http://www.mcponline.org) contains supplemental material.

[d] Both authors contributed equally to this work.

[e] A New Investigator of the Heart and Stroke Foundation of Canada and a Canada Research Chair in Cardiovascular Proteomics and Molecular Therapeutics. To whom correspondence may be addressed: Charles H. Best Inst., University of Toronto, 112 College St., Toronto, Ontario M5G 1L6, Canada. Tel.: 416-978-5609; Fax: 416-978-8528; E-mail: anthony.gramolini@utoronto.ca.

[f] A Canada Research Chair in Proteomics of Cancer Research. Present address: Ontario Cancer Inst., Division of Cancer Genomics and Proteomics, University of Toronto, Toronto, Ontario M5G IL7, Canada.

[k] A Career Investigator with the Heart and Stroke Foundation of Ontario.

[l] The Ontario Research Chair in Biomarkers. To whom correspondence may be addressed: Donnelly Centre for Cellular and Biomedical Research, University of Toronto, 160 College St., Toronto, Ontario M5S 3E1, Canada. Tel.: 416-946-7281; Fax: 416-978-7437; E-mail: andrew.emili@utoronto.ca.

REFERENCES

1. Thom, T., Haase, N., Rosamond, W., Howard, V. J., Rumsfeld, J., Manolio, T., Zheng, Z. J., Flegal, K., O'Donnell, C., Kittner, S., Lloyd-Jones, D., Goff, D. C., Jr., Hong, Y., Adams, R., Friday, G., Furie, K., Gorelick, P., Kissela, B., Marler, J., Meigs, J., Roger, V., Sidney, S., Sorlie, P., Steinberger, J., Wasserthiel-Smoller, S., Wilson, M., and Wolf, P. (2006) Heart disease and stroke statistics—2006 update: a report from the American Heart Association Statistics Committee and Stroke Statistics Subcommittee. *Circulation* **113,** e85–e151

2. Molkentin, J. D., Lu, J. R., Antos, C. L., Markham, B., Richardson, J., Robbins, J., Grant, S. R., and Olson, E. N. (1998) A calcineurin-dependent transcriptional pathway for cardiac hypertrophy. *Cell* **93,** 215–228
3. Huss, J. M., and Kelly, D. P. (2005) Mitochondrial energy metabolism in heart failure: a question of balance. *J. Clin. Investig.* **115,** 547–555
4. Dorn, G. W., II, and Force, T. (2005) Protein kinase cascades in the regulation of cardiac hypertrophy. *J. Clin. Investig.* **115,** 527–537
5. Morita, H., Seidman, J., and Seidman, C. E. (2005) Genetic causes of human heart failure. *J. Clin. Investig.* **115,** 518–526
6. Benjamin, I. J., and Schneider, M. D. (2005) Learning from failure: congestive heart failure in the postgenomic age. *J. Clin. Investig.* **115,** 495–499
7. Schmitt, J. P., Kamisago, M., Asahi, M., Li, G. H., Ahmad, F., Mende, U., Kranias, E. G., MacLennan, D. H., Seidman, J. G., and Seidman, C. E. (2003) Dilated cardiomyopathy and heart failure caused by a mutation in phospholamban. *Science* **299,** 1410–1413
8. Zvaritch, E., Backx, P. H., Jirik, F., Kimura, Y., de Leon, S., Schmidt, A. G., Hoit, B. D., Lester, J. W., Kranias, E. G., and MacLennan, D. H. (2000) The transgenic expression of highly inhibitory monomeric forms of phospholamban in mouse heart impairs cardiac contractility. *J. Biol. Chem.* **275,** 14985–14991
9. Crackower, M. A., Oudit, G. Y., Kozieradzki, I., Sarao, R., Sun, H., Sasaki, T., Hirsch, E., Suzuki, A., Shioi, T., Irie-Sasaki, J., Sah, R., Cheng, H. Y., Rybin, V. O., Lembo, G., Fratta, L., Oliveira-dos-Santos, A. J., Benovic, J. L., Kahn, C. R., Izumo, S., Steinberg, S. F., Wymann, M. P., Backx, P. H., and Penninger, J. M. (2002) Regulation of myocardial contractility and cell size by distinct PI3K-PTEN signaling pathways. *Cell* **110,** 737–749
10. Crackower, M. A., Sarao, R., Oudit, G. Y., Yagil, C., Kozieradzki, I., Scanga, S. E., Oliveira-dos-Santos, A. J., da Costa, J., Zhang, L., Pei, Y., Scholey, J., Ferrario, C. M., Manoukian, A. S., Chappell, M. C., Backx, P. H., Yagil, Y., and Penninger, J. M. (2002) Angiotensin-converting enzyme 2 is an essential regulator of heart function. *Nature* **417,** 822–828
11. Oudit, G. Y., Trivieri, M. G., Khaper, N., Husain, T., Wilson, G. J., Liu, P., Sole, M. J., and Backx, P. H. (2004) Taurine supplementation reduces oxidative stress and improves cardiovascular function in an iron-overload murine model. *Circulation* **109,** 1877–1885
12. Gramolini, A. O., Trivieri, M. G., Oudit, G. Y., Kislinger, T., Li, W., Patel, M. M., Emili, A., Kranias, E. G., Backx, P. H., and Maclennan, D. H. (2006) Cardiac-specific overexpression of sarcolipin in phospholamban null mice impairs myocyte function that is restored by phosphorylation. *Proc. Natl. Acad. Sci. U. S. A.* **103,** 2446–2451
13. Trivieri, M. G., Oudit, G. Y., Sah, R., Kerfant, B. G., Sun, H., Gramolini, A. O., Pan, Y., Wickenden, A. D., Croteau, W., Morreale de Escobar, G., Pekhletski, R., St Germain, D., Maclennan, D. H., and Backx, P. H. (2006) Cardiac-specific elevations in thyroid hormone enhance contractility and prevent pressure overload-induced cardiac dysfunction. *Proc. Natl. Acad. Sci. U. S. A.* **103,** 6043–6048
14. Kislinger, T., Rahman, K., Radulovic, D., Cox, B., Rossant, J., and Emili, A. (2003) PRISM, a generic large scale proteomic investigation strategy for mammals. *Mol. Cell. Proteomics* **2,** 96–106
15. Kislinger, T., Gramolini, A. O., MacLennan, D. H., and Emili, A. (2005) Multidimensional protein identification technology (MudPIT): technical overview of a profiling method optimized for the comprehensive proteomic investigation of normal and diseased heart tissue. *J. Am. Soc. Mass. Spectrom.* **16,** 1207–1220
16. Kislinger, T., Cox, B., Kannan, A., Chung, C., Hu, P., Ignatchenko, A., Scott, M. S., Gramolini, A. O., Morris, Q., Hallett, M. T., Rossant, J., Hughes, T. R., Frey, B., and Emili, A. (2006) Global survey of organ and organelle protein expression in mouse: combined proteomic and transcriptomic profiling. *Cell* **125,** 173–186
17. Gramolini, A. O., Kislinger, T., Liu, P., MacLennan, D. H., and Emili, A. (2006) Analyzing the cardiac muscle proteome by liquid chromatography mass spectrometry-based expression proteomics. *Methods Mol. Biol.* **357,** 15–31
18. Eng, J. K., McCormack, A. L., and Yates, J. R. (1994) An approach to correlate tandem mass spectral data of peptides with amino acid sequences in a protein database. *J. Am. Soc. Mass Spectrom.* **5,** 976–989
19. Liu, H., Sadygov, R. G., and Yates, J. R., III (2004) A model for random sampling and estimation of relative protein abundance in shotgun proteomics. *Anal. Chem.* **76,** 4193–4201
20. Cleveland, W. S., Grosse, E., and Shyu, W. M. (1992) Local regression models, in *Statistical Models in S* (Chambers, J. M., and Hastie, T. J., eds) pp. 309-376, Wadsworth & Brooks/Cole, Pacific Grove, CA
21. Benjamin, I. J., and Hochberg, Y. (1995) Controlling the false discovery rate: a practical and powerful approach to multiple testing. *J. R. Stat. Soc.* **57,** 289–300
22. Hochberg, Y., and Benjamini, Y. (1990) More powerful procedures for multiple significance testing. *Stat. Med.* **9,** 811–818
23. Culhane, A. C., Perriere, G., and Higgins, D. G. (2003) Cross-platform comparison and visualisation of gene expression data using co-inertia analysis. *BMC Bioinformatics* **4,** 59
24. Cox, B., Kislinger, T., Wigle, D. A., Kannan, A., Brown, K., Okubo, T., Hogan, B., Jurisica, I., Frey, B., Rossant, J., and Emili, A. (2007) Integrated proteomic and transcriptomic profiling of mouse lung development and Nmyc target genes. *Mol. Syst. Biol.* **3,** 109
25. Gramolini, A. O., Burton, E. A., Tinsley, J. M., Ferns, M. J., Cartaud, A., Cartaud, J., Davies, K. E., Lunde, J. A., and Jasmin, B. J. (1998) Muscle and neural isoforms of agrin increase utrophin expression in cultured myotubes via a transcriptional regulatory mechanism. *J. Biol. Chem.* **273,** 736–743
26. Gramolini, A. O., and Jasmin, B. J. (1999) Expression of the utrophin gene during myogenic differentiation. *Nucleic Acids Res.* **27,** 3603–3609
27. Nakai, K., and Horton, P. (1999) PSORT: a program for detecting sorting signals in proteins and predicting their subcellular localization. *Trends Biochem. Sci.* **24,** 34–36
28. Chen, Y., Zhang, Y., Yin, Y., Gao, G., Li, S., Jiang, Y., Gu, X., and Luo, J. (2005) SPD—a web-based secreted protein database. *Nucleic Acids Res.* **33,** D169–D173
29. Zhang, Y., Zhang, Y., Adachi, J., Olsen, J. V., Shi, R., de Souza, G., Pasini, E., Foster, L. J., Macek, B., Zougman, A., Kumar, C., Wisniewski, J. R., Jun, W., and Mann, M. (2007) MAPU: Max-Planck Unified database of organellar, cellular, tissue and body fluid proteomes. *Nucleic Acids Res.* **35,** D771–D779
30. Omenn, G. S., States, D. J., Adamski, M., Blackwell, T. W., Menon, R., Hermjakob, H., Apweiler, R., Haab, B. B., Simpson, R. J., Eddes, J. S., Kapp, E. A., Moritz, R. L., Chan, D. W., Rai, A. J., Admon, A., Aebersold, R., Eng, J., Hancock, W. S., Hefta, S. A., Meyer, H., Paik, Y. K., Yoo, J. S., Ping, P., Pounds, J., Adkins, J., Qian, X., Wang, R., Wasinger, V., Wu, C. Y., Zhao, X., Zeng, R., Archakov, A., Tsugita, A., Beer, I., Pandey, A., Pisano, M., Andrews, P., Tammen, H., Speicher, D. W., and Hanash, S. M. (2005) Overview of the HUPO Plasma Proteome Project: results from the pilot phase with 35 collaborating laboratories and multiple analytical groups, generating a core dataset of 3020 proteins and a publicly-available database. *Proteomics* **5,** 3226–3245
31. States, D. J., Omenn, G. S., Blackwell, T. W., Fermin, D., Eng, J., Speicher, D. W., and Hanash, S. M. (2006) Challenges in deriving high-confidence protein identifications from data gathered by a HUPO plasma proteome collaborative study. *Nat. Biotechnol.* **24,** 333–338
32. von Harsdorf, R., Edwards, J. G., Shen, Y. T., Kudej, R. K., Dietz, R., Leinwand, L. A., Nadal-Ginard, B., and Vatner, S. F. (1997) Identification of a cis-acting regulatory element conferring inducibility of the atrial natriuretic factor gene in acute pressure overload. *J. Clin. Investig.* **100,** 1294–1304
33. Vikstrom, K. L., Bohlmeyer, T., Factor, S. M., and Leinwand, L. A. (1998) Hypertrophy, pathology, and molecular markers of cardiac pathogenesis. *Circ. Res.* **82,** 773–778
34. McConnell, B. K., Fatkin, D., Semsarian, C., Jones, K. A., Georgakopoulos, D., Maguire, C. T., Healey, M. J., Mudd, J. O., Moskowitz, I. P., Conner, D. A., Giewat, M., Wakimoto, H., Berul, C. I., Schoen, F. J., Kass, D. A., Seidman, C. E., and Seidman, J. G. (2001) Comparison of two murine models of familial hypertrophic cardiomyopathy. *Circ. Res.* **88,** 383–389
35. De Celle, T., Vanrobaeys, F., Lijnen, P., Blankesteijn, W. M., Heeneman, S., Van Beeumen, J., Devreese, B., Smits, J. F., and Janssen, B. J. (2005) Alterations in mouse cardiac proteome after in vivo myocardial infarction: permanent ischaemia versus ischaemia-reperfusion. *Exp. Physiol.* **90,** 593–606
36. Arber, S., Hunter, J. J., Ross, J., Jr., Hongo, M., Sansig, G., Borg, J., Perriard, J. C., Chien, K. R., and Caroni, P. (1997) MLP-deficient mice exhibit a disruption of cardiac cytoarchitectural organization, dilated cardiomyopathy, and heart failure. *Cell* **88,** 393–403
37. Chien, K. R. (1999) Stress pathways and heart failure. *Cell* **98,** 555–558
38. Sano, M., Minamino, T., Toko, H., Miyauchi, H., Orimo, M., Qin, Y., Aka-

zawa, H., Tateno, K., Kayama, Y., Harada, M., Shimizu, I., Asahara, T., Hamada, H., Tomita, S., Molkentin, J. D., Zou, Y., and Komuro, I. (2007) p53-induced inhibition of Hif-1 causes cardiac dysfunction during pressure overload. *Nature* **446,** 444–448
39. Ron, D. (2002) Translational control in the endoplasmic reticulum stress response. *J. Clin. Investig.* **110,** 1383–1388
40. Okada, K., Minamino, T., Tsukamoto, Y., Liao, Y., Tsukamoto, O., Takashima, S., Hirata, A., Fujita, M., Nagamachi, Y., Nakatani, T., Yutani, C., Ozawa, K., Ogawa, S., Tomoike, H., Hori, M., and Kitakaze, M. (2004) Prolonged endoplasmic reticulum stress in hypertrophic and failing heart after aortic constriction: possible contribution of endoplasmic reticulum stress to cardiac myocyte apoptosis. *Circulation* **110,** 705–712
41. Kerkela, R., Grazette, L., Yacobi, R., Iliescu, C., Patten, R., Beahm, C., Walters, B., Shevtsov, S., Pesant, S., Clubb, F. J., Rosenzweig, A., Salomon, R. N., Van Etten, R. A., Alroy, J., Durand, J. B., and Force, T. (2006) Cardiotoxicity of the cancer therapeutic agent imatinib mesylate. *Nat. Med.* **12,** 908–916
42. Xu, C., Bailly-Maitre, B., and Reed, J. C. (2005) Endoplasmic reticulum stress: cell life and death decisions. *J. Clin. Investig.* **115,** 2656–2664
43. Hamada, H., Suzuki, M., Yuasa, S., Mimura, N., Shinozuka, N., Takada, Y., Suzuki, M., Nishino, T., Nakaya, H., Koseki, H., and Aoe, T. (2004) Dilated cardiomyopathy caused by aberrant endoplasmic reticulum quality control in mutant KDEL receptor transgenic mice. *Mol. Cell. Biol.* **24,** 8007–8017
44. Berridge, M. J., Bootman, M. D., and Roderick, H. L. (2003) Calcium signalling: dynamics, homeostasis and remodelling. *Nat. Rev. Mol. Cell Biol.* **4,** 517–529
45. Adachi, J., Kumar, C., Zhang, Y., Olsen, J. V., and Mann, M. (2006) The human urinary proteome contains more than 1500 proteins, including a large proportion of membrane proteins. *Genome Biol.* **7,** R80
46. Schirmer, E. C., and Gerace, L. (2005) The nuclear membrane proteome: extending the envelope. *Trends Biochem. Sci.* **30,** 551–558
47. Washburn, M. P., Wolters, D., and Yates, J. R., III (2001) Large-scale analysis of the yeast proteome by multidimensional protein identification technology. *Nat. Biotechnol.* **19,** 242–247
48. Mootha, V. K., Bunkenborg, J., Olsen, J. V., Hjerrild, M., Wisniewski, J. R., Stahl, E., Bolouri, M. S., Ray, H. N., Sihag, S., Kamal, M., Patterson, N., Lander, E. S., and Mann, M. (2003) Integrated analysis of protein composition, tissue diversity, and gene regulation in mouse mitochondria. *Cell* **115,** 629–640
49. Mootha, V. K., Lindgren, C. M., Eriksson, K. F., Subramanian, A., Sihag, S., Lehar, J., Puigserver, P., Carlsson, E., Ridderstrale, M., Laurila, E., Houstis, N., Daly, M. J., Patterson, N., Mesirov, J. P., Golub, T. R., Tamayo, P., Spiegelman, B., Lander, E. S., Hirschhorn, J. N., Altshuler, D., and Groop, L. C. (2003) PGC-1α-responsive genes involved in oxidative phosphorylation are coordinately downregulated in human diabetes. *Nat. Genet.* **34,** 267–273
50. Beausoleil, S. A., Jedrychowski, M., Schwartz, D., Elias, J. E., Villen, J., Li, J., Cohn, M. A., Cantley, L. C., and Gygi, S. P. (2004) Large-scale characterization of HeLa cell nuclear phosphoproteins. *Proc. Natl. Acad. Sci. U. S. A.* **101,** 12130–12135
51. Krapfenbauer, K., Fountoulakis, M., and Lubec, G. (2003) A rat brain protein expression map including cytosolic and enriched mitochondrial and microsomal fractions. *Electrophoresis* **24,** 1847–1870
52. Foster, L. J., de Hoog, C. L., Zhang, Y., Zhang, Y., Xie, X., Mootha, V. K., and Mann, M. (2006) A mammalian organelle map by protein correlation profiling. *Cell* **125,** 187–199
53. Barth, A. S., Kuner, R., Buness, A., Ruschhaupt, M., Merk, S., Zwermann, L., Kaab, S., Kreuzer, E., Steinbeck, G., Mansmann, U., Poustka, A., Nabauer, M., and Sultmann, H. (2006) Identification of a common gene expression signature in dilated cardiomyopathy across independent microarray studies. *J. Am. Coll. Cardiol.* **48,** 1610–1617
54. Steenbergen, C., Afshari, C. A., Petranka, J. G., Collins, J., Martin, K., Bennett, L., Haugen, A., Bushel, P., and Murphy, E. (2003) Alterations in apoptotic signaling in human idiopathic cardiomyopathic hearts in failure. *Am. J. Physiol.* **284,** H268–H276
55. Hwang, J. J., Allen, P. D., Tseng, G. C., Lam, C. W., Fananapazir, L., Dzau, V. J., and Liew, C. C. (2002) Microarray gene expression profiles in dilated and hypertrophic cardiomyopathic end-stage heart failure. *Physiol. Genomics* **10,** 31–44
56. Dos Remedios, C. G., Liew, C. C., Allen, P. D., Winslow, R. L., Van Eyk, J. E., and Dunn, M. J. (2003) Genomics, proteomics and bioinformatics of human heart failure. *J. Muscle Res. Cell Motil.* **24,** 251–260
57. Stanley, B. A., Gundry, R. L., Cotter, R. J., and Van Eyk, J. E. (2004) Heart disease, clinical proteomics and mass spectrometry. *Dis. Markers* **20,** 167–178
58. McGregor, E., and Dunn, M. J. (2003) Proteomics of heart disease. *Hum. Mol. Genet.* **12,** R135–R144
59. Banfi, C., Brioschi, M., Wait, R., Begum, S., Gianazza, E., Fratto, P., Polvani, G., Vitali, E., Parolari, A., Mussoni, L., and Tremoli, E. (2006) Proteomic analysis of membrane microdomains derived from both failing and non-failing human hearts. *Proteomics* **6,** 1976–1988
60. Dohke, T., Wada, A., Isono, T., Fujii, M., Yamamoto, T., Tsutamoto, T., and Horie, M. (2006) Proteomic analysis reveals significant alternations of cardiac small heat shock protein expression in congestive heart failure. *J. Card. Fail.* **12,** 77–84
61. Faber, M. J., Agnetti, G., Bezstarosti, K., Lankhuizen, I. M., Dalinghaus, M., Guarnieri, C., Caldarera, C. M., Helbing, W. A., and Lamers, J. M. (2006) Recent developments in proteomics: implications for the study of cardiac hypertrophy and failure. *Cell Biochem. Biophys.* **44,** 11–29
62. Lindsey, M. L., Goshorn, D. K., Comte-Walters, S., Hendrick, J. W., Hapke, E., Zile, M. R., and Schey, K. (2006) A multidimensional proteomic approach to identify hypertrophy-associated proteins. *Proteomics* **6,** 2225–2235
63. Pan, Y., Kislinger, T., Gramolini, A. O., Zvaritch, E., Kranias, E. G., MacLennan, D. H., and Emili, A. (2004) Identification of biochemical adaptations in hyper- or hypocontractile hearts from phospholamban mutant mice by expression proteomics. *Proc. Natl. Acad. Sci. U. S. A.* **101,** 2241–2246
64. Marciniak, S. J., and Ron, D. (2006) Endoplasmic reticulum stress signaling in disease. *Physiol. Rev.* **86,** 1133–1149
65. Yano, M., Ikeda, Y., and Matsuzaki, M. (2005) Altered intracellular Ca^{2+} handling in heart failure. *J. Clin. Investig.* **115,** 556–564
66. Boyce, M., Bryant, K. F., Jousse, C., Long, K., Harding, H. P., Scheuner, D., Kaufman, R. J., Ma, D., Coen, D. M., Ron, D., and Yuan, J. (2005) A selective inhibitor of eIF2α dephosphorylation protects cells from ER stress. *Science* **307,** 935–939
67. Magnusson, C., Libelius, R., and Tagerud, S. (2003) Nogo (Reticulon 4) expression in innervated and denervated mouse skeletal muscle. *Mol. Cell. Neurosci.* **22,** 298–307
68. Masuda, H., Tanaka, K., Takagi, M., Ohgami, K., Sakamaki, T., Shibata, N., and Takahashi, K. (1996) Molecular cloning and characterization of human non-smooth muscle calponin. *J. Biochem.* (*Tokyo*) **120,** 415–424
69. Doll, D., Sarikas, A., Krajcik, R., and Zolk, O. (2007) Proteomic expression analysis of cardiomyocytes subjected to proteasome inhibition. *Biochem. Biophys. Res. Commun.* **353,** 436–442
70. Sasaki, H., Dai, M., Auclair, D., Fukai, I., Kiriyama, M., Yamakawa, Y., Fujii, Y., and Chen, L. B. (2001) Serum level of the periostin, a homologue of an insect cell adhesion molecule, as a prognostic marker in nonsmall cell lung carcinomas. *Cancer* **92,** 843–848
71. Siriwardena, B. S., Kudo, Y., Ogawa, I., Kitagawa, M., Kitajima, S., Hatano, H., Tilakaratne, W. M., Miyauchi, M., and Takata, T. (2006) Periostin is frequently overexpressed and enhances invasion and angiogenesis in oral cancer. *Br. J. Cancer* **95,** 1396–1403